Xiang *et al.*
Chinese Journal of Mechanical Engineering (2022) 35:38
https://doi.org/10.1186/s10033-022-00704-5

Chinese Journal of Mechanical Engineering

ORIGINAL ARTICLE

Open Access

Heat Transfer Performance and Structural Optimization of a Novel Micro-channel Heat Sink

Jianhua Xiang[1*], Liangming Deng[1], Chao Zhou[1], Hongliang Zhao[1], Jiale Huang[1,2] and Sulian Tao[3]

Abstract

With the advent of the 5G era, the design of electronic equipment is developing towards thinness, intelligence and multi-function, which requires higher cooling performance of the equipment. Micro-channel heat sink is promising for the heat dissipation of super-thin electronic equipment. In this study, thermal resistance theoretical model of the micro-channel heat sink was first established. Then, fabrication process of the micro-channel heat sink was introduced. Subsequently, heat transfer performance of the fabricated micro-channel heat sink was tested through the developed testing platform. Results show that the developed micro-channel heat sink has more superior heat dissipation performance over conventional metal solid heat sink and it is well suited for high power LEDs application. Moreover, the micro-channel structures in the heat sink were optimized by orthogonal test. Based on the orthogonal optimization, heat dissipation performance of the micro-channel radiator was further improved.

Keywords: Micro-channel, Phase change heat sink, Heat transfer performance testing, Finite element simulation, Orthogonal test

1 Introduction

The problem of heat dissipation is the crux that restricts the development of LED. How to design an excellent LED heat dissipation system is an urgent problem which needs to be solved in the LED industry. Generally, there are two steps for LED chip cooling technology as follows: The heat is firstly conducted from LED chip to heat sink through heat pipe. Then, the heat is dissipated to ambient environment through external heat sink [1–4]. The inadequacy of this kind of heat dissipation system is the overweight of lamps and lanterns due to the large mass of external heat sink. In addition, some LEDs operate outdoors, resulting in unstable factors such as corrosion and damage. Active heat dissipation technology is another solution for LED heat dissipation. The use of external power such as pumps and fans can enhance heat convection to improve the heat transfer coefficient of the radiator surface. However, packaging is troublesome for this kind of heat dissipation system because of external pumps or fans. Moreover, noise will be generated and not easy to be controlled. Because of the advantages of simple structure, reliable operation and good thermal conductivity, heat pipe is widely used in the field of LED heat dissipation. Kim et al. [5] applied heat pipes to high-power LED and found that the heat dissipation effect of chips with heat pipes was better than that without heat pipes at the same wind speed. In the case of heat pipe cooling system, the total thermal resistance of is between 1.8–2.71 K/W. Chen et al. [6] integrated flat heat pipe into the LED heat dissipation system. When the flat heat pipe is simplified as a heat conduction plate with high thermal conductivity, simulation results are consistent with the experiments. The maximum difference of thermal expansion temperature rise is 6.3% and the overall temperature uniformity is good.

*Correspondence: xiangjh@gzhu.edu.cn
[1] School of Mechanical and Electrical Engineering, Guangzhou University, Guangzhou 510006, China
Full list of author information is available at the end of the article

Micro-channel heat dissipation is also a promising technology. The heat dissipation principle is similar to that of heat pipe, but the conduction modes of these two devices are different. Heat pipe refers to one-dimensional linear heat conduction, while the heat in micro-channel radiator is conducted on a two-dimensional surface, thus higher heat conduction efficiency can be achieved. To be specific, the liquid at the bottom of the vacuum chamber absorbs heat from the chip and evaporates quickly. Then, the steam diffuses in the vacuum chamber and then condenses into liquid when it is in contact with the fins (cold side). The processes of evaporation and condensation, which are similar to that of refrigerator, circulate rapidly in a micro-channel heat sink and the high heat dissipation efficiency can be achieved.

In 1981, Tuckerman and Pease proposed the concept of micro-channel heat sink and applied it into the heat dissipation of very-large-scale integrated circuits (VLSI) [7]. After that, more researches have been directed into this field. Representatively, Serizawa et al. [8] examined gas-liquid two-phase flow patterns in micro-channels using a microscope and found that two-phase flow patterns are sensitive to the surface conditions of the inner wall. Bladimir et al. [9] adopted the method of entropy generation minimization to optimize the micro-channels and a lower flow resistance was obtained. Jajja et al. [10] investigated the influence of fin spacing on the cooling performance of mini-channel heat sinks and found that fins with 0.2 mm spacing produced the lowest base temperature at a power of 325 W. Khoshvaght-Aliabadi et al. [11, 12] investigated the cooling performance of sinusoidal-wavy mini-channel heat sink (SWMCHS) by experiment and found that a decrease of wave length or an increase of wave amplitude can improve its thermal performance. Imran et al. [13] investigated serpentine mini-channel heat sink through numerical and experimental methods. Results showed that two inlets and two outlets can improve the performance of serpentine mini-channel heat sink. Drummond et al. [14] developed a hierarchical manifold micro-channel heat sink array which obtained very high heat removal rate. Kumar et al. [15] investigated heat transfer and pressure drop characteristics of micro-channel which uses Al_2O_3 nanofluid and Al_2O_3-MWCNT hybrid nanofluid as cooling medium by numerical and experimental methods. Ho et al. [16] investigated thermal characteristics of divergent rectangular mini-channel heat sinks and found that diverging the mini-channels leads to the reduction of thermal resistance at high flow rates. Hajmohammadi et al. [17] investigated nanofluid-cooled double-layered micro-channel heat sink. Optimal design of the heat sink is achieved. Other researchers have also contributed to this field [18–21].

In this study, thermal resistance theoretical model of the micro-channel radiator was first established. Then, the fabrication process of the micro-channel radiator was introduced. Subsequently, heat transfer performance of the fabricated micro-channel heat sink was tested through the developed testing platform. Results show that the developed micro-channel heat sink has more superior cooling performance over conventional metal solid heat sink and it is well suited for high power LEDs. Moreover, the micro-channel structures in the heat sink were optimized by orthogonal test. Based on the orthogonal optimization, heat dissipation performance of the micro-channel radiator was further improved.

2 Theoretical Model

As it is shown in Figure 1, thermal resistance of the developed LED micro-channel cooling system can be divided into the following parts. ① Thermal resistance between LED PN junction and the solder layer, R_1; ② Thermal resistance between the solder layer and the aluminum substrate, R_2; ③ Thermal resistance between the aluminum substrate and thermal conductive adhesive, R_3; ④ Thermal resistance of the heat sink, R_4; ⑤ Convective thermal resistance between the surface of micro-channel heat sink and the surrounding environment, R_5. In addition, the temperature of LED chip is denoted by T_C (℃) and environment temperature is denoted by T_A (℃). For convenience, the thermal resistance can also be divided into two aspects, i.e. internal thermal resistance that encapsulated within the lamps and lanterns, R_{in}, and external thermal resistance that produced by the heat sink and environment, R_{out}. It is obvious that internal heat resistance includes R_1, R_2 and R_3, while external heat resistance includes R_4 and R_5. From the above, thermal resistance of the whole cooling system can be calculated as

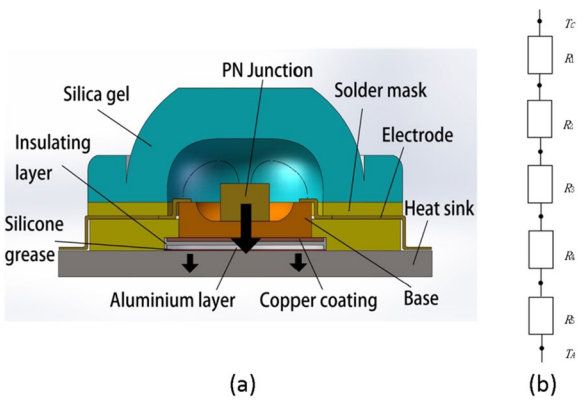

Figure 1 **a** LED cooling system and **b** its corresponding thermal resistance network

$$R_{Total} = R_{in} + R_{out} = R_1 + R_2 + R_3 + R_4 + R_5, \quad (1)$$

where

$$R_4 = \frac{1}{\overline{h} \cdot A}, \quad (2)$$

$$R_5 = \frac{T_W - T_\infty}{Q - Q_\theta}, \quad (3)$$

$$Q_\theta = \varepsilon \cdot \sigma \cdot A \cdot \left(T_W^4 - T_\infty^4\right), \quad (4)$$

$$R_{out} = R_4 + R_5 = \frac{T_W - T_\infty}{Q - Q_\theta} + \frac{1}{\overline{h} \cdot A}, \quad (5)$$

where $\overline{h}$ is the average convective heat transfer coefficient of the surface of micro-channel heat sink (W/m^2/K), A is the superficial area of micro-channel heat sink (m^2), T_W is the surface temperature of the heat sink (℃), Q_θ is quantity of radiation heat (W), ε is the radiance of the micro-channel heat sink.

Suppose the efficiency of thermoelectric conversion is 80%,

$$T_C = T_\infty + Q \cdot R_{Total} \cdot 80\% = T_\infty + R_{Total} \cdot V \cdot I \cdot 80\%, \quad (6)$$

where Q is input power of the chip, V is the voltage of the circuit, and I is the current of the circuit.

To ensure normal and stable operation of LEDs, i.e. to reduce the junction temperature of the chip, R_{Total}, that consists of R_{in} and R_{out} has to be reduced. R_{in} is reduced by using new materials and new packaging technology that is difficult to implement. So what we are most concerned about is to reduce R_{out}. This is the emphasis of this study, i.e. to reduce thermal resistance of the heat sink and convective thermal resistance between the surface of micro-channel heat sink and the surrounding environment (R_4 and R_5), by structure optimization of micro-channel heat sink.

3 Fabrication and Heat Transfer Performance Testing

3.1 Fabrication of the Micro-channel Heat Sink

First, two pieces of aluminum sheets having the same size and thickness were provided. Second, micro-channels were etched onto one single piece of aluminum sheet. Then, two pieces were accurately aligned and riveted together. Subsequently, the riveted plates were heated to a certain temperature and welded together through the diffusion welding. Due to the effect of recrystallization, two pieces turned into one singe composite board. Finally, high-pressure fluid (working fluid) was injected into the specimen along the etched micro-channel, forming the thermal conductive loop. The working fluid was injected through the filling port, and then the micro-channel heat sink was vacuumed through the filling port. Finally, it was sealed by welding.

In consideration of high power LED working conditions, the mixture of water and R134a (i.e. tetrafluoroethane) was selected as working fluid. Before liquid injection, the cavity volume inside the microchannel heat sink was calculated. The fill ratio is then obtained by dividing the volume of the injected working fluid by the total volume of internal cavity. The filling ratio was set as 20%, which is accepted by most scholars [22–24]. To further improve the cooling performance of micro-channel heat sink, the surface of the heat sink was processed with sand blasting and black oxide treatment to increase surface emissivity. The fabricated micro-channel heat sink with the size of 380 mm × 200 mm × 16 mm is shown in Figure 2.

3.2 Heat Transfer Performance Testing of the Micro-channel Heat Sink

The heat transfer performance testing platform consists of the data acquisition module, the heating module and the micro-channel heat sink etc., as it is shown in Figure 3. The data acquisition module consists of Advantech USB-4718 DAQ Card, data cable, thermocouples and a computer etc. In this study, T type thermocouples were applied and connected to the data acquisition card. The measured temperature can be stored on a computer in real time. The heating module consists of the Bakelite, an aluminium block and heating rods to replace the LED chip, as it is shown in Figure 4. Four blind holes were drilled into the aluminium block to place heating rods. The working power of every single heating rod is up to 100 W. Bakelite in the heating system has the effect of heat preservation and insulation. In the absence of

Figure 2 The front and back of the fabricated micro-channel heat sink

Figure 3 The heat transfer performance testing platform

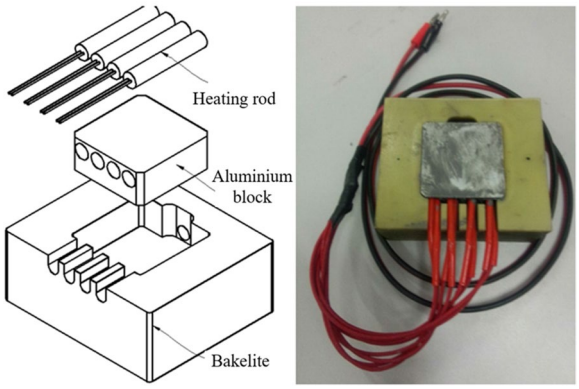

Figure 4 The heating module

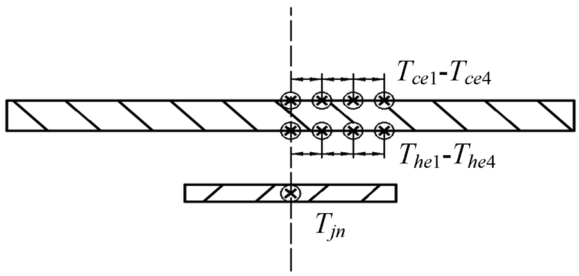

Figure 5 The layout of thermocouples

Bakelite insulation, experimental measurement temperature will be lower than the actual temperature. A pair of thermocouple is placed at the center of every heating rod to measure the simulated LED chip junction temperature. In order to eliminate the clearance between the heating module and heat sink, a thin layer of thermal conductive silicone was evenly coated on the surface of the aluminium block.

The layout of the thermocouples is exhibited in Figure 5. In detail, a pair of thermocouples is arranged at the center of the heating rod to measure the simulated junction temperature of LED, denoted as T_{jn}. On the surface where the micro-channel radiator is in contact with the heat source (hot side), four pairs of thermocouples are evenly distributed along the radial direction from the center point, denoted as T_{he1}–T_{he4}, respectively. To measure the temperature of the honeycomb side (cold side) of the micro-channel radiator, four pairs of thermocouples are arranged opposite to T_{he1}–T_{he4}, denoted as T_{ce1}–T_{ce4}, respectively. In addition, a pair of thermocouples is applied to measure the ambient temperature T_a.

The uncertainty of the system is mainly manifested in the output power error and thermocouple temperature measurement error. The errors of power supply are ±10 mV and ±1 mA. The measurement accuracy of thermocouple temperature is 0.5%.

4 Experimental Results and Discussions

4.1 Comparison of Micro-channel Radiator with Conventional Metal Solid Heat Sink

First of all, in order to verify heat dissipation performance of the micro-channel radiator, a set of comparative experiments were conducted. A piece of aluminium plate with the same size and shape as the micro-channel radiator was applied for heat dissipation. Heating power of 90 W was applied to these two specimens (aluminium plate and micro-channel radiator). After the temperature of the radiators remained steady, these two specimens were photographed using infrared imager, as shown in Figure 6. The plot shows that the micro-channel radiator reduces the chip temperature by 15.6 ℃ (the maximum temperature reduces from 97.9 ℃ to 82.3 ℃) under the same circumstance, suggesting its great heat dissipation performance.

The relationship between the temperatures at the center of the heat sink (i.e., T_{he1}) and time under different input powers is shown in Figure 7. Figure 7a shows that the temperature increases quickly at the early stage and

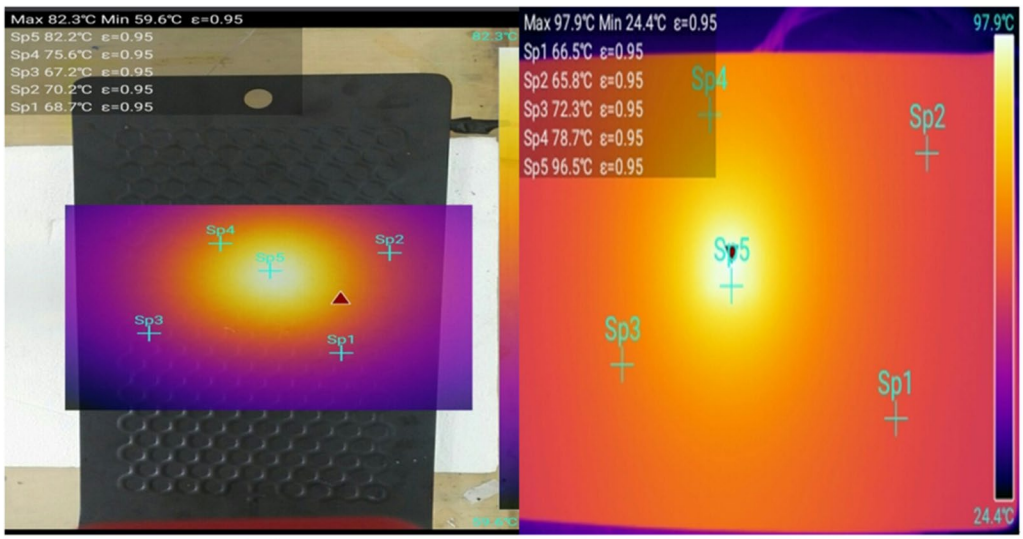

Figure 6 Temperature distribution in **a** the micro-channel radiator and **b** an aluminium plate under the same input power of 90 W

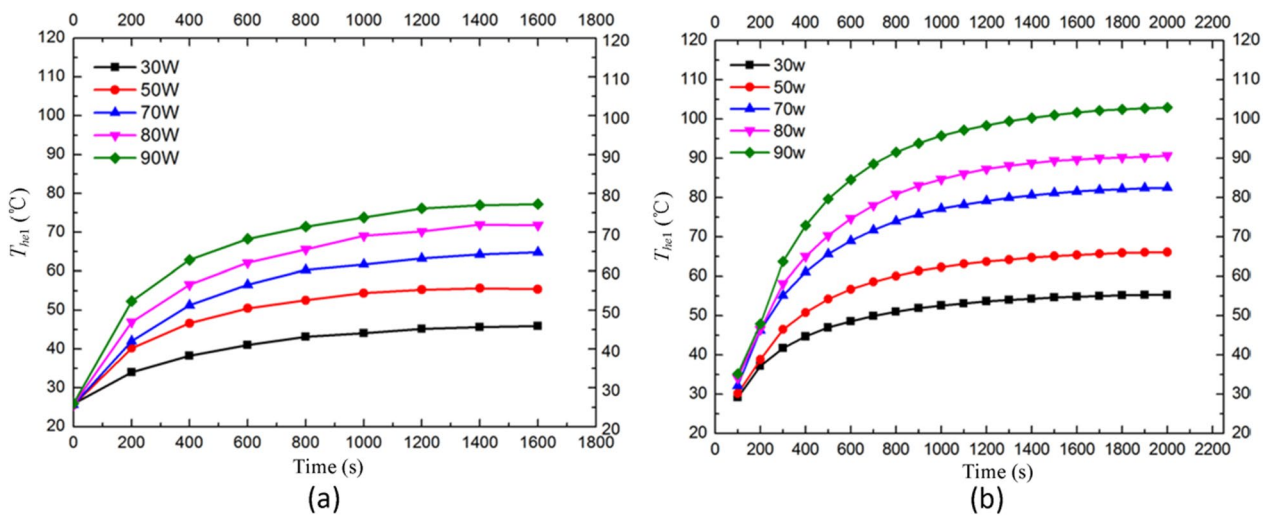

Figure 7 Temperature at the center of the heat sink (T_{he1}) with time duration in **a** the micro-channel radiator and **b** an aluminium plate

then remains steady not until 20 min. Figure 7b shows that the temperature increases all the time, and cannot get a balance in 30 min. The fast response of micro-channel radiator is attributed to the phase change heat dissipation. Generally, the time to reach thermal balance is to measure the start-up performance of a radiator. Thus, the developed micro-channel radiator has a great start-up heat transfer performance.

The relationship between the temperature of thermal source (i.e., T_{jn}) and time under different input powers is shown in Figure 8. The tendency is consistent with the temperature change at the central point of heat sink (Figure 7). Few fluctuations indicate that the overall stability is good. At the start-up stage of micro-channel radiator, the cooling requirements can be well satisfied. In contrast, when it comes to conventional aluminum radiator, the temperature has been rising and continues to increase over 100 ℃. This is due to the fact that, the micro-channel radiator contains heat transfer working medium inside, and heat transfer capacity of phase transition is much higher than heat conduction. Consequently, the micro-channel radiator can reach the

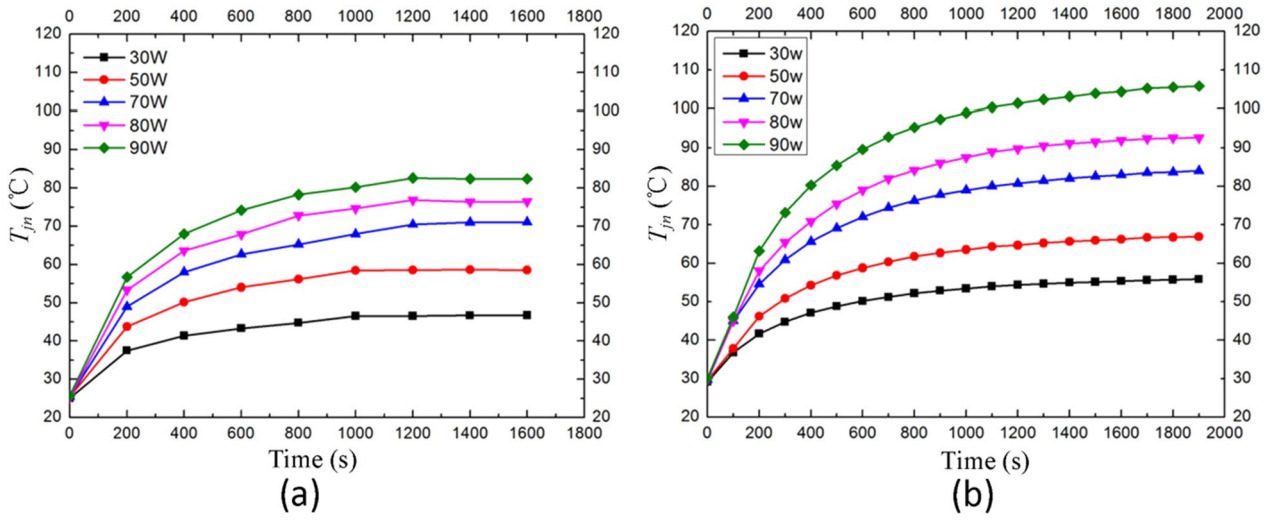

Figure 8 Temperature of thermal source (T_{jn}) with time duration in **a** the micro-channel radiator and **b** an aluminium plate

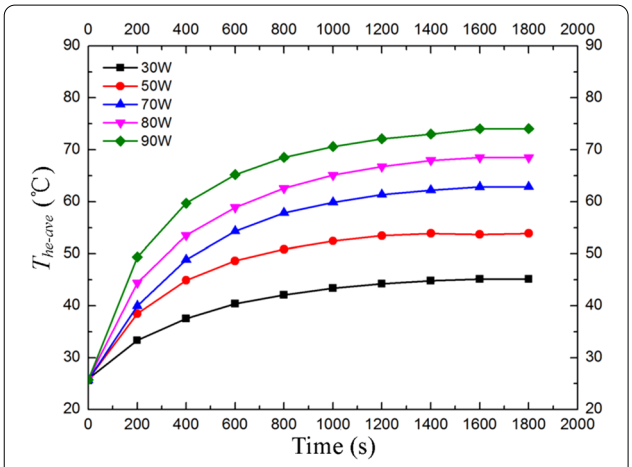

Figure 9 Average temperature of the hot side ($T_{he\text{-}ave}$) of the micro-channel heat sink with time duration

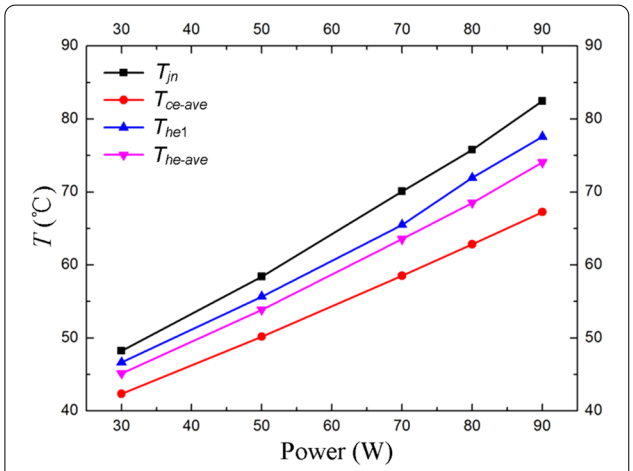

Figure 10 Temperature of typical measurement points under different input powers

balance faster than the conventional aluminum plate radiator, and the chip temperature can be lowered greatly.

In addition, the relationship between average temperature of the hot side of the micro-channel heat sink (i.e., $T_{he\text{-}ave}$) and time under different input powers are shown in Figure 9. To make a comparison, the correlations of the temperature at the center of the heat sink T_{he1}, the temperature of thermal source T_{jn}, average temperature of the hot side of micro-channel heat sink $T_{he\text{-}ave}$, and average temperature of the cold side of micro-channel heat sink $T_{ce\text{-}ave}$ with different input powers are combined to Figure 10. It can be seen that the overall trend of four curves is consistent. All the temperatures increase with the increase of input power, and few fluctuations can be found. The highest temperature is less than 85 ℃, which can satisfy the requirement of LEDs.

4.2 Thermal Resistances of Micro-channel Radiator under Different Input Powers

As it is denoted in Figure 5, relevant thermal resistances of micro-channel radiator can be calculated as follows.

$$R_c = \frac{T_{jn} - T_{he}}{Q_h}, \tag{7}$$

where R_c is thermal contact resistance, T_{he} is the temperature of the center of the micro-channel radiator, that is equal to T_{he1}, and Q_h is heating power.

$$T_{he-ave} = \frac{T_{he1} + T_{he2} + T_{he3} + T_{he4}}{4}, \tag{8}$$

where $T_{he\text{-}ave}$ is the average temperature of the hot side of the micro-channel radiator.

$$R_{ave} = \frac{T_{he1} - T_{he-ave}}{Q_h}, \tag{9}$$

where R_{ave} is the heat diffusion resistance.

$$T_{ce-ave} = \frac{T_{ce1} + T_{ce2} + T_{ce3} + T_{ce4}}{4}, \tag{10}$$

where $T_{\text{ce-ave}}$ is the average temperature of cold side of micro-channel radiator.

$$R_{heat-\sin k} = \frac{T_{he-ave} - T_{ce-ave}}{Q_h}, \tag{11}$$

where $R_{heat\text{-}\sin k}$ is the thermal resistance of micro-channel heat sink.

$$R_{ch} = \frac{T_{ce-ave} - T_a}{Q_h}, \tag{12}$$

where R_{ch} is the thermal convection resistance of the surface of heat sink.

$$R_{Total} = \frac{T_{jn} - T_a}{Q_h}, \tag{13}$$

where R_{Total} is the total thermal resistance of micro-channel radiator.

Thermal resistances calculated by the Eqs. (7), (9) and (11)–(13) under different input powers are shown in Figure 11. The plot shows that the sequence of thermal resistances of each part is as follows: thermal convection resistance of the surface of heat sink > thermal resistance of the micro-channel heat sink > thermal contact resistance > heat diffusion resistance. There are few changes of thermal resistance of the heat sink, thermal contact resistance and heat diffusion resistance with the increase of heating power. However, the effect of heating power onto thermal convective resistance is relatively large. It is seen that with the increase of heating power thermal convective resistance become smaller. This is mainly because the surface temperature of micro-channel radiator increases with the increase of heating power, resulting in a stronger thermal radiation and heat convection of the surface of the micro-channel radiator. As a result, thermal convective resistance of the surface of the micro-channel radiator is reduced. It should be pointed out that, to further reduce the junction temperature of the chip, thermal convective resistance of the surface of the micro-channel radiator should be further reduced by the optimization of surface structure.

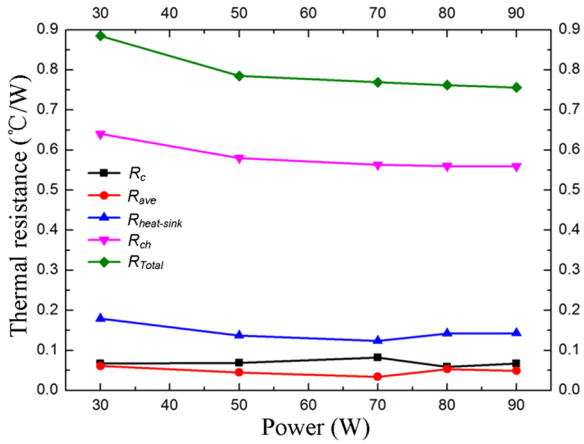

Figure 11 Thermal resistances under different input powers

5 Numerical Simulation and Structural Optimization

5.1 Numerical Simulation

In this study, FLUENT is applied to simulate the heat transfer performance of the developed micro-channel radiators. In light of huge computation burden, several simplifications have been made: (1) Two-dimensional numerical models are established instead of the complicated three-dimensional honeycomb structures; (2) High power LED chips are simplified as planar heat source with the same area; (3) The material of the micro-channel radiator is isotropic and the thermo-physical property is constant.

The numerical model is shown in Figure 12(a), in which green color represents the micro-channels. Fine mesh is generated in the channels, as shown in Figure 12(b). After grid division, the quality of the grid has been checked. It is found that although the number of grids in the model is large, the quality is positive. Multiphase-mixture model is selected as the physical model. The material of the radiator is defined as *Al*6063, while the working fluid is the mixture of water and R134a. Subsequently, PISO algorithm is selected to solve the equations.

The steady-state temperature contour is shown in Figure 13(a) when the ambient temperature is 25 ℃ and the LED chip power is 90 W. The plot shows that the temperature of the micro-channel is homogeneous with a gradual transition.

To make a comparison between numerical simulation and experiment, the temperature contour of

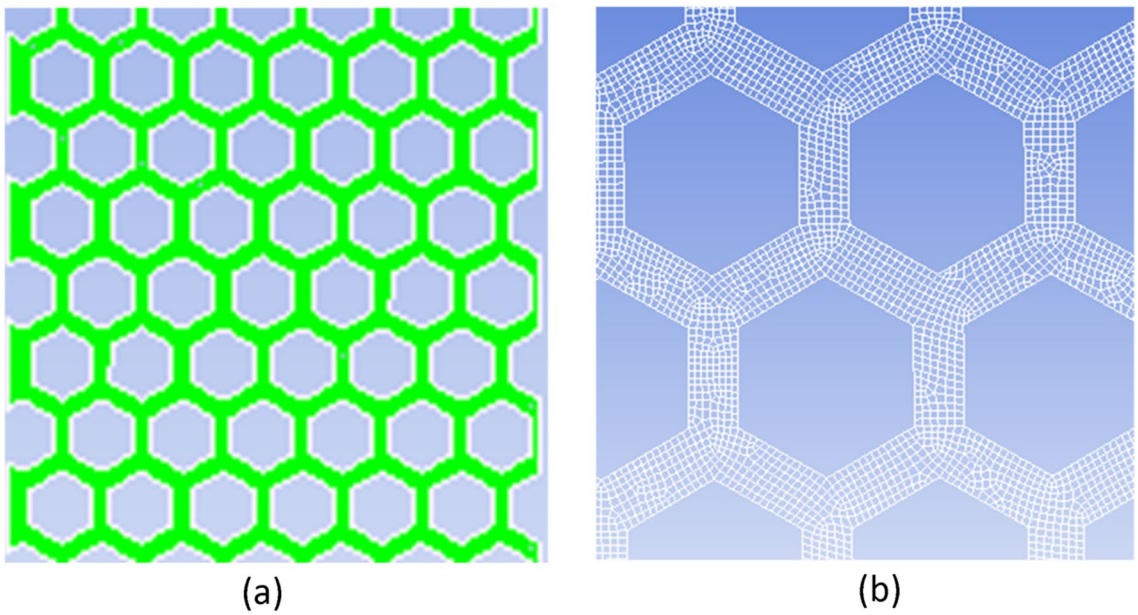

Figure 12 **a** FE model, and **b** fine mesh of the micro-channels

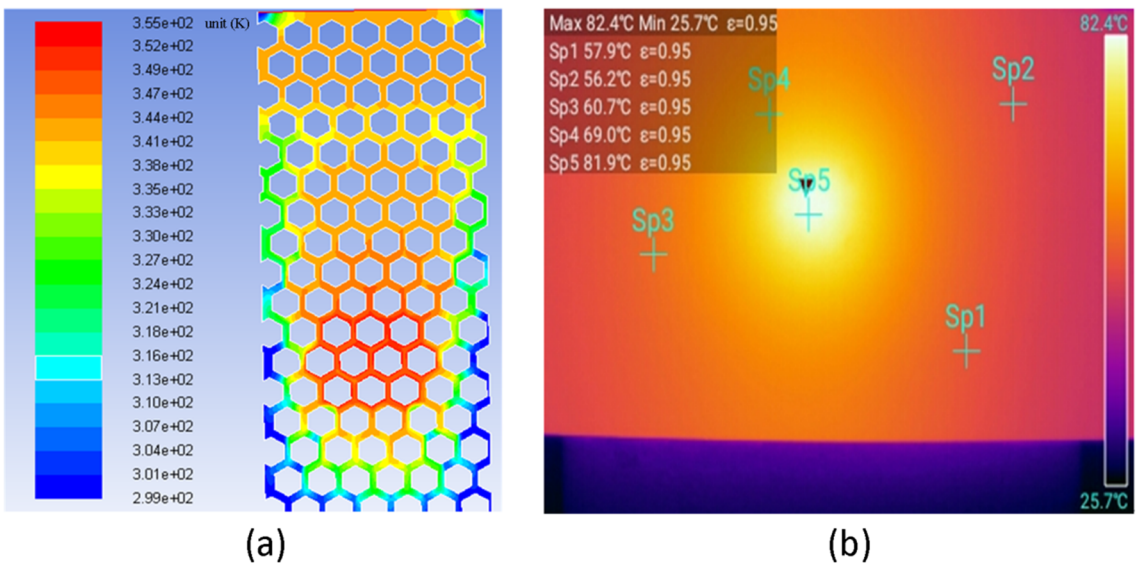

Figure 13 Temperature contour of the micro-channel heat sink from **a** FE simulation and **b** experiment

the specimen under the input power of 90 W is photographed using infrared imager as shown in Figure 13(b). Sp1 to sp5 refer to 5 typical measurement points, while ε is emissivity. The highest temperature from simulation is $(355-273.15)=81.85$ ℃, corresponding to the 82.4 ℃ in the experiment. The lowest temperature is $(299-273.15)=25.85$ ℃, corresponding to the 25.7 ℃ in the experiment. Upon the comparison, the simulated result coincides well with that of experiment.

Figure 14(a) displays the velocity distribution image of heat transfer working medium in the micro-channel. The plot shows that the velocity of the working medium, which is close to the heat source, is larger than that away from the heat source. There is no eddy current present on the whole, indicating that the channels

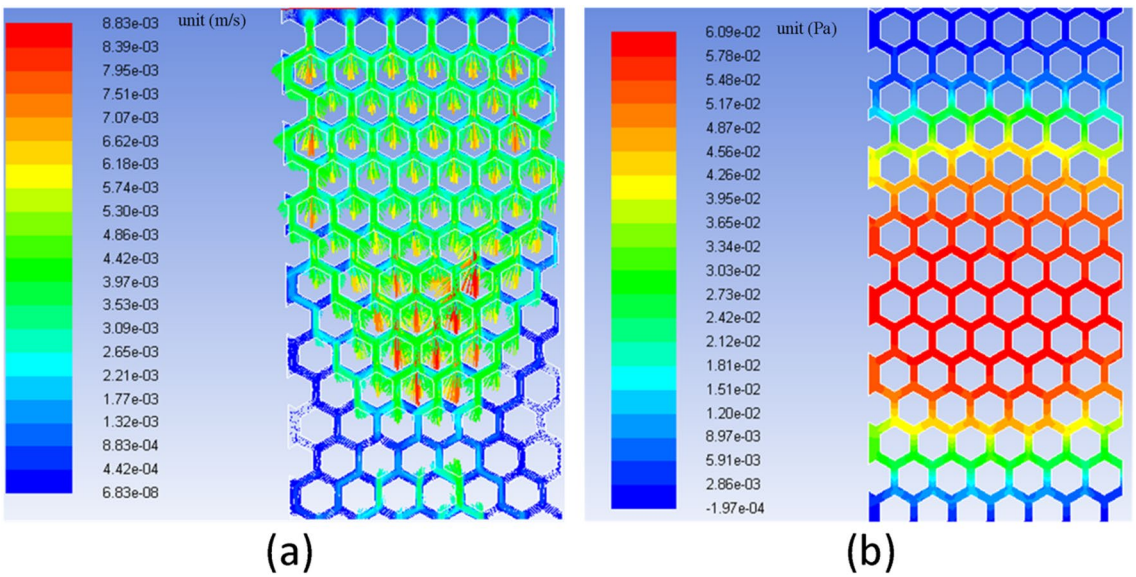

Figure 14 **a** Velocity distribution image, and **b** pressure distribution image of the micro-channel heat sink from FE simulation

are unobstructed. Figure 14(b) displays the internal pressure distribution image in the micro-channel. It can be seen that the pressure of the area close to the heat source is large, while the pressure of the area away from the heat source is small, consistent with common sense.

5.2 Structural Optimization

In order to achieve the best heat dissipation performance, orthogonal experiment is applied to optimize the micro-channel structures. As it is shown in Table 1, four factors including honeycomb type (A), distance between adjacent honeycombs (B), honeycomb depth (C) and circumcircle radius of polygons (D) are selected in this orthogonal experiment. There are four levels for each factor, resulting in a 4-factor 4-level test. In this regard, a type of L16 (4^5) orthogonal array is selected, as shown in Table 2, in which one more blank column is added.

Sixteen finite element models are established whose structural parameters are presented in Table 2. FLUENT is then applied to simulate the heat transfer performance of each model with the same procedures introduced in Section 5.1. In terms of the simulated junction temperature of LED chips from 16 cases, the results of orthogonal test are obtained and shown in Table 3. In Table 3, S_i ($i=1, 2, 3, 4$) is calculated as

$$S_i = \sum T_j, \tag{14}$$

where j is the test number (row number) having a factor level of i. For example, S_3 in column C (corresponding to the depth of 1.5 mm) is calculated as $S_3=84.87+83.09+79.55+80.67=328.18$, which corresponds to the test number of $3^{\#}$,$8^{\#}$,$9^{\#}$ and $14^{\#}$, respectively.

Then, s_i is obtained by

$$s_i = \frac{S_i}{n}, \tag{15}$$

where n is the number of factors, i.e. four in this study. For example, s_3 is calculated as $s_3=S_3/4=328.18/4=82.05$.

Then, range R is calculated as

Table 1 Factors and levels

Factors	Honeycomb type *A*	Distance between honeycombs *B* (mm)	Honeycomb depth *C* (mm)	Circum-radius of polygons *D* (mm)
1#	Regular triangle	2	0.5	5
2#	Square	4	1	6
3#	Circle	6	1.5	7
4#	Regular Hexagon	8	2	8

Table 2 Orthogonal array of L16 (4^5)

Test number	Honeycomb type *A*	Distance between honeycombs *B* (mm)	Honeycomb depth *C* (mm)	Circum-radius of polygons *D* (mm)	Blank column
1#	1	1	1	1	1
2#	1	2	2	2	2
3#	1	3	3	3	3
4#	1	4	4	4	4
5#	2	1	2	3	4
6#	2	2	1	4	3
7#	2	3	4	1	2
8#	2	4	3	2	1
9#	3	1	3	4	2
10#	3	2	4	3	1
11#	3	3	1	2	4
12#	3	4	2	1	3
13#	4	1	4	2	3
14#	4	2	3	1	4
15#	4	3	2	4	1
16#	4	4	1	3	2

Table 3 The results of orthogonal test

Test number	Honeycomb type *A*	Distance between honeycombs *B*(mm)	Honeycomb depth *C*(mm)	Circum-radius of polygons *D* (mm)	Blank column	Simulated results *T* (℃)
1#	1	1	1	1	1	81.13
2#	1	2	2	2	2	82.05
3#	1	3	3	3	3	84.87
4#	1	4	4	4	4	87.39
5#	2	1	2	3	4	82.77
6#	2	2	1	4	3	80.36
7#	2	3	4	1	2	83.58
8#	2	4	3	2	1	83.09
9#	3	1	3	4	2	79.55
10#	3	2	4	3	1	80.91
11#	3	3	1	2	4	84.57
12#	3	4	2	1	3	87.05
13#	4	1	4	2	3	80.32
14#	4	2	3	1	4	80.67
15#	4	3	2	4	1	81.83
16#	4	4	1	3	2	81.46
S_1	335.44	323.77	327.52	332.43		
S_2	329.8	323.99	333.7	330.03		
S_3	332.08	334.85	328.18	330.01		
S_4	324.28	338.99	332.2	329.13		
s_1	83.86	80.94	81.88	83.11		
s_2	82.45	81.00	83.43	82.51		
s_3	83.02	83.71	82.05	82.50		
s_4	81.07	84.75	83.05	82.28		
R	2.79	3.81	1.55	0.83		
factors	B→A→C→D					

$$R = \max\{S_1, S_2, S_3, S_4\} - \min\{S_1, S_2, S_3, S_4\}. \quad (16)$$

It should be noted that larger R means greater effect onto the result of experiment. Therefore, the order of influence of these four factors in turn is $B \rightarrow A \rightarrow C \rightarrow D$, with R of 3.81, 2.79, 1.55 and 0.83, respectively.

The ultimate aim of the orthogonal test is to get the combination with the lowest temperature. Therefore, the selection criterion should be the minimum S_i value, leading to a minimum junction temperature of LED chips. In this study,

Factor A: $S_1 > S_3 > S_2 > S_4$
Factor B: $S_4 > S_3 > S_2 > S_1$
Factor C: $S_2 > S_4 > S_3 > S_1$
Factor D: $S_1 > S_2 > S_3 > S_4$

Consequently, the best structural parameters for the micro-channel should be *A*4*B*1*C*1*D*4, i.e. the type of honeycomb is regular hexagon, the distance between adjacent honeycombs is 2 mm, the depth of honeycomb is 0.5 mm and the circum-radius of regular hexagon is 8 mm.

The simulated temperature contour of the micro-channel heat sink with the best combination (*A*4*B*1*C*1*D*4) is shown in Figure 15. The maximum temperature in this Figure is $(350 - 273.15) = 76.85$ ℃, lower than the maximum temperature of 79.55 ℃ from the combination of 9#. Obviously, upon the orthogonal optimization, heat dissipation performance of the micro-channel radiator is further improved.

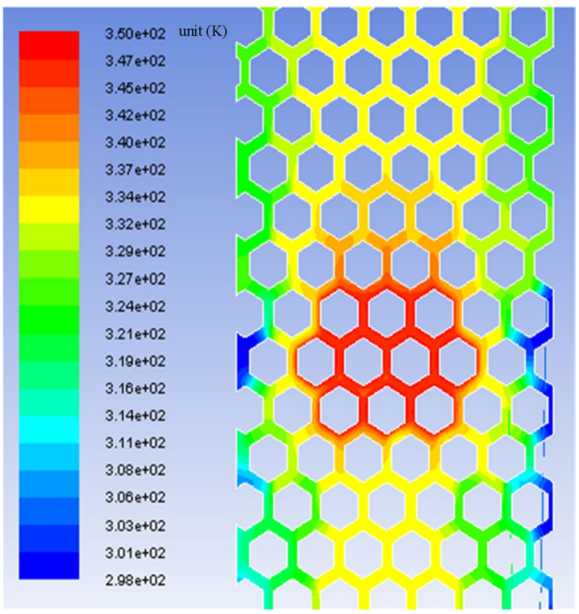

Figure 15 Temperature contour of the micro-channel heat sink with the best combination (*A*4*B*1*C*1*D*4)

6 Conclusions

A thermal resistance theoretical model of the micro-channel radiator was first established. Subsequently, the fabrication process of the micro-channel radiator was introduced. Heat transfer performance of the fabricated micro-channel heat sink was tested through the developed testing platform. Results show that:

1) The developed micro-channel heat sink has more superior cooling performance over conventional metal solid heat sink and it is well suited for high power LEDs.
2) The micro-channel structures in the heat sink were optimized by orthogonal test, and the heat dissipation performance of the micro-channel radiator was further improved.
3) The best structural parameters for the micro-channel are as follows: the type of honeycomb is regular hexagon, the distance between adjacent honeycombs is 2 mm, the depth of honeycomb is 0.5 mm and the circum-radius of regular hexagon is 8 mm.

Acknowledgments
Not applicable.

Authors' Contributions
JX and LD did the thermal performance tests and data analysis. HZ and JH wrote the manuscript. CZ and ST revised the manuscript. All authors read and approved the final manuscript.

Authors' Information
Jianhua Xiang, born in 1978, is currently a professor at *School of Mechanical and Electrical Engineering*, *Guangzhou University*, *China*. His research interests include design and manufacture of high-performance thermal control device and microstructure precision forming.

Liangming Deng is currently a master candidate at *School of Mechanical and Electrical Engineering*, *Guangzhou University*, *China*.

Chao Zhou is currently a lecturer at *School of Mechanical and Electrical Engineering*, *Guangzhou University*, *China*. His research interests focus on ultrasonic non-destructive testing.

Hongliang Zhao received his master degree in *Guangzhou University*, *China*, in 2018.

Jiale Huang is currently an associate professor at *School of Mechanical and Electrical Engineering*, *Guangzhou University*, *China*. His research interests include design and manufacture of high-performance thermal control device and bionic structural design.

Sulian Tao is currently a professor at *Guangdong Technical College of Water Resources and Electric Engineering*, *China*. Her research interests include optimal design and manufacture of microstructures.

Funding
Supported by the National Natural Science Foundation of China (Grant Nos. 51975135 and 52005422), Guangzhou Science and Technology Project (Grant No. 201707010429) and Special Innovation Projects of Universities in Guangdong Province (Grant No. 2018GKTSCX085).

Competing Interests
The authors declare no competing financial interests.

Author Details
[1]School of Mechanical and Electrical Engineering, Guangzhou University, Guangzhou 510006, China. [2]Department of Mechanical and Electrical Engineering, Xiamen University, Xiamen 361005, China. [3]Department of Mechanical Engineering, Guangdong Technical College of Water Resources and Electric Engineering, Guangzhou 510925, China.

Received: 7 October 2020 Revised: 9 March 2022 Accepted: 22 March 2022
Published online: 11 April 2022

References

[1] S J Park, D Jang, K S Lee. Thermal performance improvement of a radial heat sink with a hollow cylinder for LED downlight applications. *International Journal of Heat and Mass Transfer*, 2015, 89: 1184-1199.
[2] B Li, C Byon. Orientation effects on thermal performance of radial heat sinks with a concentric ring subject to natural convection. *International Journal of Heat and Mass Transfer*, 2015, 90: 102-108.
[3] Y Wu, Y Tang, Z Li, et al. Experimental investigation of a PCM-HP heat sink on its thermal performance and anti-thermal-shock capacity for high-power LEDs. *Applied Thermal Engineering*, 2016, 108: 192-203.
[4] J Xiang, C Zhou, C Zhang, et al. Optimization of three-dimensional boiling enhancement structure at evaporation surface for high power light emitting diode. *Transactions of Nonferrous Metals Society of China*, 2018, 28: 1404-1412.
[5] K Lan, J H Choi, H J Sun, et al. Thermal analysis of LED array system with heat pipe. *Thermochimica Acta*, 2007, 455(1): 21-25.
[6] Y S Chen, K H Chien, T C Hung, et al. Numerical simulation of a heat sink embedded with a vapor chamber and calculation of effective thermal conductivity of a vapor chamber. *Applied Thermal Engineering*, 2009, 29(13): 2655-2664.
[7] D B Tuckerman, R F W. Pease. High-performance heat sinking for VLSI. *IEEE Electron Device Letters*, 1981, 2(5): 126-129.
[8] A Serizawa, Z Feng, Z Kawara. Two-phase flow in microchannels. *Experimental Thermal and Fluid Science*, 2002, 26: 703-714.
[9] R A Bladimir, B Feng, G P Peterson. Comparison and optimization of single-phase liquid cooling devices for the heat dissipation of high-power LED arrays. *Applied Thermal Engineering*, 2013, 59: 648-659.
[10] S A Jajja, W Ali, H M Ali, et al. Water cooled minichannel heat sinks for microprocessor cooling: Effect of fin spacing. *Applied Thermal Engineering*, 2014, 64: 76-82.
[11] M Khoshvaght-Aliabadi, M Sahamiyan, M Hesampour, et al. Experimental study on cooling performance of sinusoidal–wavy minichannel heat sink. *Applied Thermal Engineering*, 2016, 92: 50-61.
[12] M Khoshvaght-Aliabadi, E Ahmadian, O Sartipzadeh. Effects of different pin-fin interruptions on performance of a nanofluid-cooled zigzag miniature heat sink (MHS). *International Communications in Heat and Mass Transfer*,2017, 81: 19-27.
[13] A A Imran, N S Mahmoud, H M Jaffal. Numerical and experimental investigation of heat transfer in liquid cooling serpentine mini-channel heat sink with different new configuration models. *Thermal Science and Engineering Progress*, 2018, 6: 128-139.
[14] K P Drummond, D Back, M D Sinanis, et al. A hierarchical manifold microchannel heat sink array for high-heat-flux two-phase cooling of electronics. *International Journal of Heat and Mass Transfer*, 2018, 117: 319-330.
[15] V Kumar, J Sarkar. Two-phase numerical simulation of hybrid nanofluid heat transfer in minichannel heat sink and experimental validation. *International Communications in Heat and Mass Transfer,* 2018, 91: 239-247.
[16] C J Ho, P C Chang, W M Yan, et al. Thermal and hydrodynamic characteristics of divergent rectangular minichannel heat sinks. *International Journal of Heat and Mass Transfer,* 2018, 122: 264–274.
[17] M R Hajmohammadi, I Toghraei. Optimal design and thermal performance improvement of a double-layered microchannel heat sink by introducing Al_2O_3 nano-particles into the water. *Physica A: Statistical Mechanics and its Applications*, 2018, 505: 328-344.
[18] A Heydari, O A Akbari, M R Safaei, et al. The effect of attack angle of triangular ribs on heat transfer of nanofluids in a microchannel. *Journal of Thermal Analysis and Calorimetry,*2018, 131: 2893-2912.
[19] Mehdi Bahiraei, Saeed Heshmatian. Thermal performance and second law characteristics of two new microchannel heat sinks operated with hybrid nanofluid containing graphene–silver nanoparticles. *Energy Conversion and Management*, 2018, 168: 357-370.
[20] T A Kingston, J A Weibel, S V Garimella. High-frequency thermal-fluidic characterization of dynamic microchannel flow boiling instabilities: Part 1 Rapid-bubble-growth instability at the onset of boiling. *International Journal of Multiphase Flow,* 2018, 106: 179-188.
[21] T V Oevelen, J A Weibel, S V Garimella. The effect of lateral thermal coupling between parallel microchannels on two-phase flow distribution. *International Journal of Heat and Mass Transfer,* 2018, 124: 769-781.
[22] Imura H, Sasaguchi K, Kozai H, et al. Critical heat flux in a closed two-phase thermosyphon. *International Journal of Heat & Mass Transfer*, 1983, 26(8): 1181-1188.
[23] Liu Z, Wang Z, Ma C. An experimental study on the heat transfer characteristics of a heat pipe heat exchanger with latent heat storage. Part II: Simultaneous charging/discharging modes. *Energy Conversion & Management*, 2006, 47(7-8): 967-991.
[24] Khandekar S, Joshi Y M, Mehta B. Thermal performance of closed two-phase thermosyphon using nanofluids. *International Journal of Thermal Sciences*, 2008, 47(6): 659-667.